ABSTRACT

HE, GUOZHEN. Microstructure Evolution and Mechanical Properties of a Heterogeneous Structured Al-5083 Alloy (Under the direction of Dr. Yuntian Zhu).

It has been a long researching goal to overcome the strength-ductility tradeoff for metals. Metals and alloys are either strong or ductile, but seldom maintain both characters for the same time. Attempts have been done by many researchers to achieve both high strength and ductility via heterogeneous structures. Here we report a heterogeneous lamella structure in 5083 aluminum alloy which is consisted of hard fine-grained domains and soft coarse-grained domains. The heterogeneous lamella structure is achieved by room-temperature rolling and partial recrystallisation.

This thesis reports the effects of annealing temperature and time on mechanical properties of Al-5083 deformed by room temperature rolling. By comparing all the data in this work and references, an optimum annealing condition is found to be 230 °C and 10 mins. Microstructures evolution is examined by TEM and EBSD. Effects of different strengthening mechanisms are discussed in this work. Back stress strengthening is believed to play the most crucial role in our samples among different strengthening mechanisms.

© Copyright 2018 Guozhen He

All Rights Reserved

Microstructure Evolution and Mechanical Properties of a Heterogeneous Structured Al-5083 Alloy

by
Guozhen He

A thesis submitted to the Graduate Faculty of
North Carolina State University
in partial fulfillment of the
requirements for the degree of
Master of Science

Materials Science and Engineering

Raleigh, North Carolina
2018

APPROVED BY:

_____	_____
Dr. Yuntian Zhu Committee Chair	Dr. Ronald Scattergood
_____	
Dr. Korukonda Murty	

BIOGRAPHY

Guozhen He was born on October 30th, 1993 in Nanjing, China. Born as a professor's child and grown up in a researchers' community in Nanjing, the influence of his family and the community has great impact on him to value modesty and diligence. Since his childhood, Guozhen has been interested in science and music. At high school, Guozhen joined a robot team and won a national prize which excited his passion in becoming a researcher and an entrepreneur.

In 2012, Guozhen attended Beihang University (Aka Beijing University of Aeronautics and Astronautics) where he found his new interest in materials science. He joined Dr. Ruixing Li's group and spent one year working on infrared shielding materials. In June 2016, Guozhen finished bachelor's degree in Materials Science and Engineering. From his research experience, Guozhen determined to pursue further study in Materials Science for future career.

Guozhen attended North Carolina State University in the department of Materials Science and Engineering in August 2016. He joined Dr. Zhu's group and started to do his researches on mechanical properties and microstructures of aluminum alloys.

ACKNOWLEDGMENTS

I would like to express my gratitude to my advisor Prof. Zhu, for his support and guidance throughout the research in the past two years. I would also like to thank Prof. Scattergood and Prof. Murty and for their precise time and patience to serve as my committee, review my thesis and presentation.

I am thankful to thank Xiaotian Fang, Ruocun Wang who helped me a lot revising the thesis, practicing presentations, and preparing for the oral exam. I would also like to thank Haotian Deng and Xinkai Ma for their advices. A thank you to all the group members for their friendship and help.

Finally, I would like to Edna Deas for her kindly help with all the paperwork and advices.

TABLE OF CONTENTS

LIST OF TABLES v
LIST OF FIGURES vi

1. Introduction 1
1.1 Statement of Purpose 1
1.2 Basics of Heterogeneous Structure 1
1.2.1 Gradient Structure 3
1.2.2 Bimodal Structure 4
1.2.3 Harmonic Structure 6
1.2.4 Nanodomained Structure 7
1.2.5 Heterogeneous Lamella Structure and Laminate Structure 8
1.3 Basics of Aluminum 5083 Alloy 11
1.4 Strengthening Mechanisms in Al-5083 Alloy 12
1.4.1 Heterogeneous Structure and Back Stress Strengthening 12
1.4.2 Grain Boundary Strengthening 14
1.4.3 Solid Solution Strengthening 16
1.4.4 Precipitation Hardening 17
1.5 Severe cold rolling of Aluminum and Aluminum Alloys 19
2. Experimental Techniques and Methods 21
2.1 Experimental Procedures 21
2.2 Back Stress Measurement 22
3. Experimental Results 24
3.1 Microstructure Characterization of Heterogeneous-Structured Al-5083 24
3.2 Mechanical Properties of Heterogenous-structured Al-5083 30
4. Discussion 35
4.1 Microstructure Evolution 35
4.2 Strengthening Mechanisms and Back Stress Strengthening in Al-5083 36
5. Conclusion 39
6. References 40

LIST OF TABLES

Table 1 Nominal composition of common commercial aluminum alloy 12

Table 2 Grain size distribution of as-rolled al-5083 with different annealing parameters 29

Table 3 Back stress of annealed al-5083 and coarse grain samples 34

LIST OF FIGURES

Figure 1 Gradient structured metal with grain sizes around 20 nm at the surface layer and coarse grains in the core [8] 3

Figure 2 Ideal schematics of bimodal grain size distributions in polycrystalline metals [28] 4

Figure 3 Schematic of a harmonic-structured material [29] 6

Figure 4 Schematic of a nanodomained Ni fabricated by electrodeposition 7

Figure 5 Schematics of an ideal lamella structure with elongated coarse grains embedded in an ultrafine-grained matrix [6] 9

Figure 6 Schematics of a typical laminate-structured material [12] 10

Figure 7 (A) Schematics of the piling up of GNDs at the interlamellar interface. (B) Plastic strain and strain gradient as the function of distance from the interface. (C) Stress as the function of function of distance from the interface [6]. (D) TEM image showing pileing-up of dislocations in a recrystallized coarse grain at tensile strain of 2% [22] 13

Figure 8 Generation of successive closed loops of dislocation line from a Frank-Read source [37] 14

Figure 9 Schematics of piling-up of dislocations from the dislocation source S1 in grain 1 under a resolved shear stress τ. S2 is a dislocation source in grain 2 [39] 15

Figure 10 Different types of serrations in a stress-strain curve 17

Figure 11 Schematics illustrating Orowan bypassing mechanism. (A) The dislocation line bows between two particles. (B) The line moves forward. [39] 18

Figure 12 Schematics showing (A) an ideal unloading-reloading stress-strain curve, (B) a real unloading-reloading cycle 22

Figure 13 TEM images of (A) equaxial grains; (B) elongated grains and isolated subgrains; (C)cell blocks and dislocation tangled zones in al-5083 with 80% rolling reduction 24

Figure 14 TEM images of (A) oval shape precipitates; (B) subgrain structures (C) elongated grains; and diffraction pattern of (D) oval shape precipitates (E) al-5083 matrix in 80% rolled 5083 with annealing at 230°C for 10 mins 25

Figure 15 EBSD image of 80% rolled 5083 samples with annealing at 230°C for 10 mins 27

Figure 16 Misorientation angles of 80% rolled 5083 samples with annealing at 230°C for 10 mins 28

Figure 17 The effects of annealing temperature on al-5083 alloy with 80% thickness reduction and annealed for 5 mins 31

Figure 18 Yield strength and uniform elongation al-5083 in this work and other data for comparison 32

Figure 19 Unloading-reloading stress-strain curve of as-rolled samples with 230°C 10min annealing 34

Figure 20 Back stress versus applied strain of as-rolled samples with 230°C 10min annealing 35

1. Introduction

1.1 Statement of Purpose

The purpose of this research is to find an efficient way to overcome the strength-ductility trade-off in a commercial aluminum 5083 alloy. One of the most efficient approach is to fabricate heterogeneous structures which exhibits a good combination of strength and ductility. In this research, we evaluated advantages and disadvantages of all the heterogeneous structures reported so far. Heterogeneous lamella structure is considered as the most ideal structure because of its high interlamellar interface density and completely constrained soft domains. Commercial aluminum 5083 (Al-5083) alloy is selected as the experimental material because of its ease of fabrication and important applications in ships and vehicle bodies. Room temperature rolling and annealing are selected to fabricate heterogeneous lamella structure. This thesis will start with introducing basic information of heterogeneous structure and features of commercial al-5083, then explain the back stress strengthening in heterogenous structures and potential methods to fabricate such structures, and finally explore the microstructure evolution and mechanical properties of heterogeneous structured al-5083.

1.2 Basics of Heterogeneous Structure

Throughout history, the progress of human society is always accompanied by a huge leap forward in materials. Metals and alloys have been playing an important role in our society for their significant mechanical properties, light weight, high conductivity, corrosion resistances, easy fabrication, and so on. Although composite materials have replaced metals in some applications such as aircraft, vehicles, and buildings [1], metals and alloys are still irreplaceable in many situations because of their ease of fabrication and tolerance of different working

conditions. It has always been a long researching goal to fabricate metallic materials with superior mechanical properties and light weight, however, strength and ductility turned out to be mutually exclusive for researches in many decades.

For the past few decades, nanostructured and ultrafined metals have raised interests of many researchers and have achieved extraordinary high yield strength, however, the ductility drops dramatically as grain size decreases to nanometer level [2–5]. With the increase in yield strength, ductility usually decreases, and vice versa. The phenomenon that ductility decreases with yield strength increase, known as strength and ductility trade-off, gradually becomes the main problem for researchers. Through decades of studies, researchers find that uniform nano- or ultrafined-structure is not able to solve this problem, thus a new strategy, which abandons the uniform structure and fabricates a heterogeneous structure for materials, becomes a promising solution to strength and ductility trade-off. Many attempts have been made to overcome the shortage of low ductile nanostructured metals and to balance the trade-off between strength and ductility. Some researches proposed a new strategy inspired by these attempts to maintain both aspects for metals at the same time. It is considered a genre of heterogeneous materials. Heterogeneous materials are defined as materials presenting huge microstructural heterogeneities in size, geometry, and strength between different domains. [6]. A heterogeneous material can be in the form of gradient structure[7–9], bimodal structure [10,11], laminate structure [12–14], harmonic structure [15,16], nanodomained structure [17], dual-phase alloys [18,19], nanotwinned grains [20,21] , and heterogeneous lamella structure [22].

1.2.1 Gradient Structure

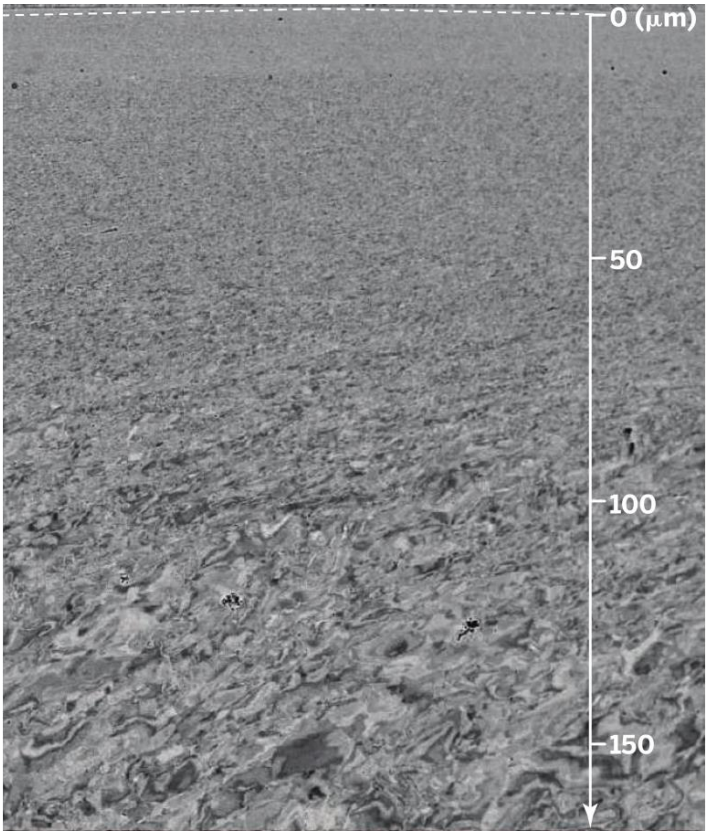

Figure 1: A typical gradient structured metal with grain sizes around 20 nm on the surface and gradually coarse grains in the core [8].

In gradient structured materials, grain sizes increase from nanoscale at the surface to micron-scale in the core [8]. The gradient structure is consisted of, in sequence, nanograins (grain size around 100nm), ultrafine grains (several hundred nm to μm), deformed coarse grains, and central coarse grain core. Nanograins at the surface can be fabricated by coating and deposition techniques such as CVD, PVD, electrodeposition, and plasma processing, however, it is hard to apply for mass production. In 2002, K.Lu's group introduced a surface mechanical attrition treatment (SMAT) to refine grains at the surface to the nanoscale, which showed good combination of yield strength and ductility [7]. SMAT is performed by shooting steel balls with

diameters around a few microns to the sample surface under different applied speeds and duration. Generally, a surface layer with grain size at nanoscale will be formed and core is still coarse-grained after SMAT. Up-to-date, SMAT has been researched to improve strength-ductility combination and fatigue behavior in different kinds of metals and alloys, such as IF steel [23], 304 Steel [24], various of aluminum alloys [25], copper [26]. In most of these works, the strength of the gradient structured materials surplus the calculation predicted by the rule of mixture (ROM) based on thicknesses of different layers [25,27].

1.2.2 Bimodal Structure

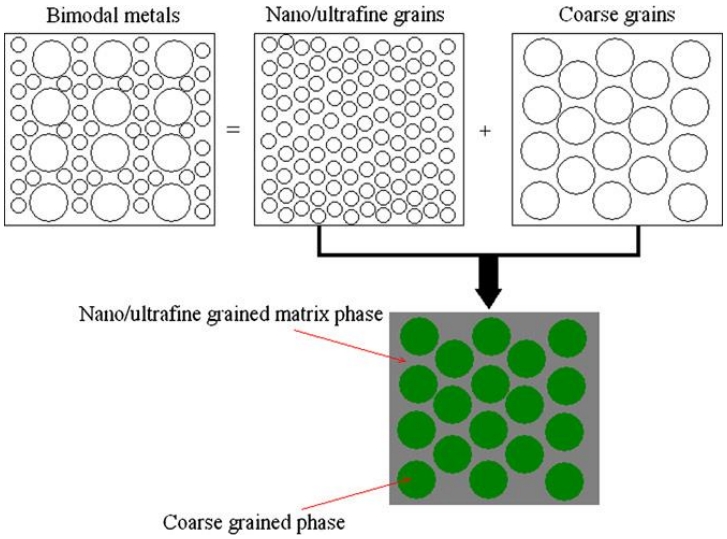

Figure 2. Ideal schematics of bimodal grain size distributions in polycrystalline metals [28].

The bimodal structure is another approach to increase tensile ductility from nanocrystalline metals. Bimodal structures were often reported in metals processed by cryo-rolling or cryo-milling [10,11,16,29]. By cryo-rolling, homogeneous materials were usually first rolled to more than 90% thickness reduction using liquid nitrogen and followed by annealing under relatively short time. Y. Wang and co-workers reported pure copper processed by cryorolling and

annealing which reached 320 MPa yield strength and 30% uniform elongation[10]. In their work, the majority of grains were in nanocrystalline to the ultrafine range. Around 25% of grains were in 1 to 3 μm. The concept of bimodal structures focused on the distribution of grains size; the ideal distribution shows a double peak for critical twinning size. The critical combination of strength and ductility for the bimodal structure materials can be achieved by double peaks in critical twinning size distribution [28]. According to Lu's research, random distribution of coarse grains and fine grains in bulk metals will not give much rise to mechanical properties [8]. In bimodal materials, it is difficult to generate strain partition and various slip systems in coarse grains and nearest nanocrystalline grains, which is the main difference from heterogeneous materials.

1.2.3 Harmonic Structure

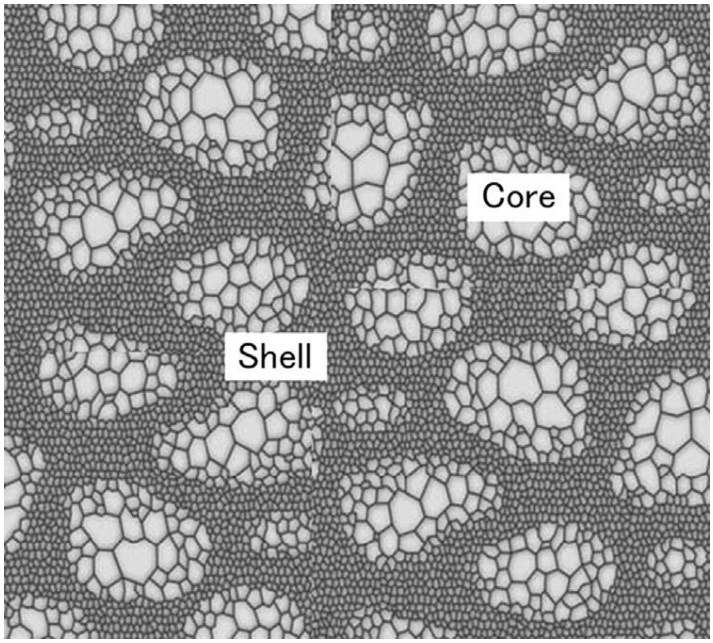

Figure 3: Schematic of a harmonic-structured material [29].

The harmonic structure was first proposed by Ameyama and co-authors[15,30]. It is a special case of the bimodal structure. Unlike a conventional bimodal structure, coarse grains around tens of microns sit as the cores in shells consisted of ultrafine grains. Harmonic structure is usually produced by mechanical milling followed by sintering [15]. The fabrication of harmonic structure has been investigated in different metals and alloys, such as pure Cu [15], pure Ti [30], Ti-Al alloys [31], and steels [29]. By tuning shell volume fraction, the best combination of yield strength and uniform elongation for different metals with harmonic structure. It is inspiring because it can produce harmonic structures in pure metals so that disturbances from other solution elements and second phases which give rise to mechanical properties can be easily ruled out in research. On the other hand, new perturbations may be introduced into the harmonic structure, for example, elements like oxygen and nitrogen may

contaminate pure metal powders during mechanical milling and sintering. What's more, the mechanical properties of harmonic structures reported so far are not superior than other structures discussed previously [15]. Taken the example of harmonic structured pure Cu, when considering the ultrafine grain framework as hard domains, the spacing between hard domain interfaces are ranging from 50 μm to 100 μm which is several times larger than the optical interface spacing [15].

1.2.4 Nanodomained Structure

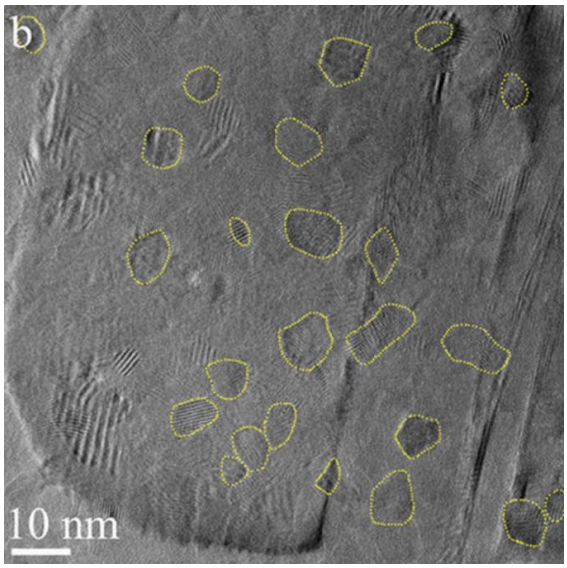

Figure 4: Schematic of a nanodomained Ni fabricated by electrodeposition.

Nanodomained structure, dual-phase steels, nanotwinned grains are special cases. In general, they are in the range of heterogenous materials, however, their heterogeneities come from effects diffetent from hard and soft domains. Nanodomained structure pure nickel was reported by X. Wu and co-authors processed via electrodeposition [17]. Around 2.4% volume fraction nanodomains (7nm in average) embedded in a matrix with average grain size around 150

nm. Their nanodomained nickel samples exhibited a yield strength almost 1.3 GPa and 30% uniform elongation while their electrodeposited ultrafine nickel samples (grain size around 200 nm) only exhibited 600 MPa yield strength and 12% uniform elongation. Unlike other heterogeneous structure, authors believed that dislocations were pinned by these nanodomains during deformation, which is similar to the scenario of the Orowan bypassing mechanism. Despite from their superb tensile test results, sample geometry (10 mm × 2.5 mm × 150 μm) in their tensile test is far from ASTM standard, which may affect their uniaxial tensile results [17]. Dual-phase alloys are another genre of heterogeneous structured materials. The heterogeneity comes from different phases in the alloys which maintain distinct elastic properties. Researches have been done with dual-phase steel, transformation induced plasticity (TRIP) steel and nanotwinned materials [9,19,20].

1.2.5 Heterogeneous Lamella Structure and Laminate Structure

Although the structures mentioned above have their unique advantages, their shortages are still obvious. In gradient materials, there are two dynamically migrating interfaces which allows dislocation density accumulation over the whole sample volume to generate large back stress. On the other hand, the effected layer of gradient materials is usually several hundred micrometers. Thus, it is hard to be utilized in thick plates, and the yield strength improvement sometimes is not sufficient. Low interface density limits the capability of back stress work hardening. It is difficult to obtain the ideal distribution of grain size in bimodal materials, causing a problematic repetition of the mechanical properties. In laminate structured materials, domain interfaces are easy to locate, which make laminate structure a good system to study interface associated properties during deformation. The disadvantage of laminate structure is that both soft domains and hard domains are subjected to same applied stress during deformation, which gives limited back stress strengthening.

Therefore, to discover a simple-fabricated HL structure and introduce more intrinsic heterogeneity inside materials become important in making heterogeneous materials. Heterogeneous lamella structure is a new and promising structure for the extraordinary combination of strength and ductility.

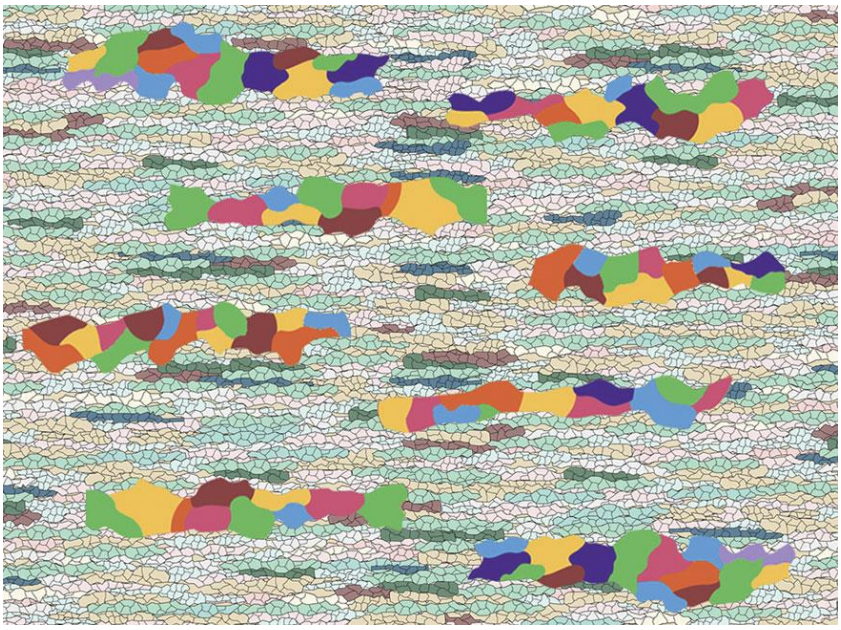

Figure 5: Schematics of an ideal lamella structure with elongated coarse grains embedded in an ultrafine-grained matrix [6].

Heterogeneous lamella (HL) structure was first reported by X.Wu and co-workers in 2015 [22]. In their work, a titanium alloy was asymmetrically rolled with 87.5% reduction, then followed by annealing at 475 °C for 5 min. According to their report, both hard domains and soft domains were formed after partial recrystallization. Hard domains were defined as areas consisted of ultrafine grains with average grain sizes around 100 nm. Soft domains were consisted of recrystallized grains with a size larger than 1 micron and were surrounded by hard domains. Their HL samples maintained the same uniform elongation as the coarse grain Ti

samples while yield strength increased 600 MPa. Soft domains deformed much more than hard domains which produced strain gradient across interlamellar interfaces. As a result, the strain gradient generated geometrically necessary dislocations which produced long-range back stress near the interfaces [22]. The authors proposed that HL structure was superior to previous bimodal structure because of its lamellar nature which gives high interlamellar interface density and completely constrained soft domains by hard domains.

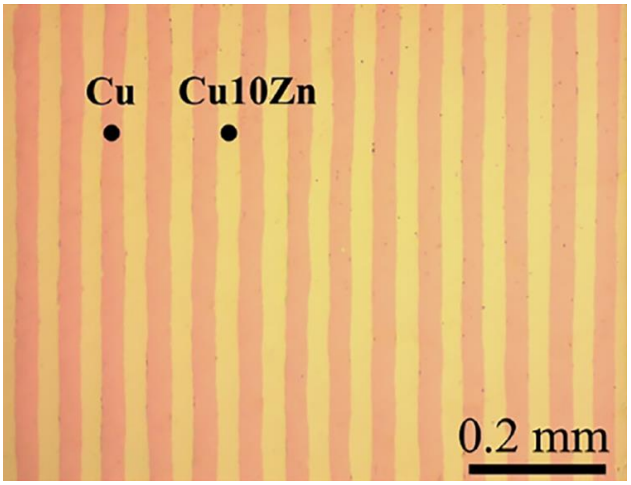

Figure 6: Schematics of a typical laminate-structured material [12].

Another method to make lamellar structure is accumulated rolling bonding (ARB) two different metals, forming a laminate structure. The laminate structure is a perfect system to study the role of the interface under deformation using either in situ or ex situ techniques. Unlike gradient heterogenous lamella structure, interfaces between soft domains and hard domains in the laminate structure are more accessible to locate because of parallel separation between different layers. C.X. Huang and coworkers researched interfaces affected zone in copper/bronze laminates [12]. They developed an in situ high-resolution digital image correlation (DIC) technique which directly proved the strain partitioning during deformation for laminate

structures. What's more, Cu and bronze share similar elastic constant but different recrystallization temperatures and stacking fault energies. These features make it easy to produce grain size heterogeneity and strain gradient. Upon deformation, geometrically necessary dislocations are always first generated in the Cu layers. These features make investigations on dislocation sources in laminates easier than in heterogenous lamella structure.

1.3 Basics of Aluminum 5083 Alloy

Magnesium is the principal alloying element in aluminum 5083 alloys with composition around 4.4 percent [32]. Aluminum 5083 is a widely used commercial alloy for ships, bridges, cars, and even missiles components. It shows good corrosion resistances and work hardening. Since global warming, air pollution, and energy shortage are becoming more and more serious issues, it's meaningful to increase yield strength and ductility simultaneously for energy efficiency purpose in all these applicationsthe . As such a popular commercial alloy, al-5083 alloy has been well studied by the material community, however, there are few reports on processing heterogeneous structures in 5083. Conventionally, possible hardening mechanisms in 5083 are as followed: solid solution strengthening, precipitation strengthening, grain boundary strengthening, and dislocation forest. It's essential to distinguish the effects of different strengthening mechanism when combining with heterogeneous structure.

Table 1: Nominal composition of common commercial aluminum alloy

AA number	Composition (%)						
	Al	Mg	Zn	Cu	Mn	Cr	other
5083	94.7	4.4	…	…	0.7	0.15	…

1.4 Strengthening Mechanisms in Al-5083 Alloy

1.4.1 Heterogeneous Structure and Back Stress Strengthening

Researchers proposed that back stress strengthening plays the most crucial role in the synergic improvement of strength and ductility for the heterogeneous structure [6,22,33]. In metals and alloys, shear flow stress is usually calculated as [34,35]

$$\tau = \alpha G b \sqrt{\rho_S + \rho_G},$$

where τ is the shear flow stress, α is an empirical constant usually ranging from 0.2-0.5, G is the shear modulus, b is the Burgers vector, ρ_S is the density of statistically stored dislocations (SSDs), ρ_G is the density of geometrically necessary dislocations (GNDs). In homogeneous materials, the contribution from geometrically necessary dislocations is usually very small, the major contribution comes from statistically stored dislocations.

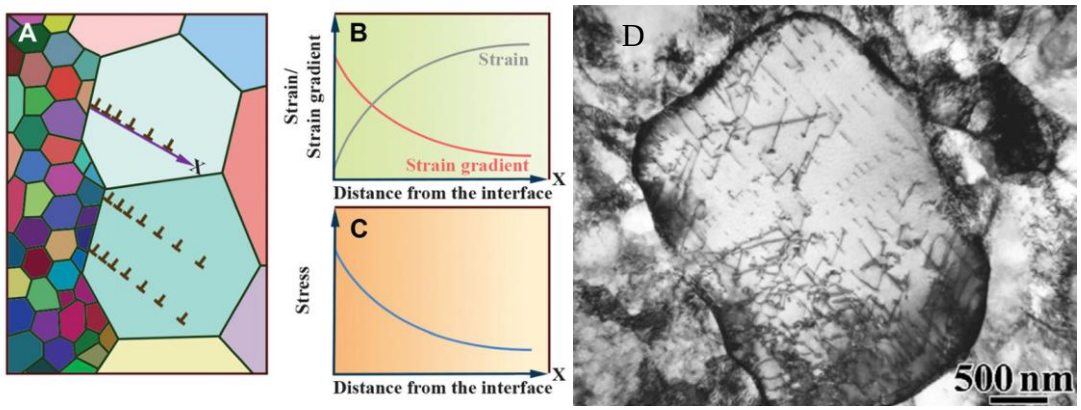

Figure 7: (A) Schematics of the piling up of GNDs at the interlamellar interface. (B) Plastic strain and strain gradient as the function of distance from the interface. (C) Stress as the function of function of distance from the interface. [6] (D) TEM image showing pileing-up of dislocations in a recrystallized coarse grain at tensile strain of 2% [22].

In heterogeneous structured materials, geometrically necessary dislocations also play an important role in strengthening. Geometrically necessary dislocations are largely generated due to effective strain gradient, when plastic strain is not homogeneous throughout the material [35]. At the same applied stress, deformation of soft domains is larger than the deformation of hard domains. When geometrically necessary dislocations are emitted from a dislocation source inside a soft domain and pile up at the interface between hard and soft domain, a long-range stress called back stress is generated [22]. In this scenario, the effective stress at the dislocation source equals to the difference between the applied stress and the back stress. It required higher applied stress to pile up more dislocations at the interface. In another scenario, the same back stress will be produced if geometrically necessary dislocations are emitted from ledge sources on the domain boundaries or the grain boundaries [12,36].

1.4.2 Grain Boundary Strengthening

Grain boundaries can act as obstacles to dislocation motions across the grains. At grain boundaries, lattices are mismatched. As a result, misfit dislocations are generated at grain boundaries to accommodate lattice misfit. Slip planes are not aligned across different grains. Dislocations cannot travel across grain boundaries upon deformation. If dislocations are generated from a Frank-Read source, they will be stopped by the grain boundary and eventually pile up with increasing plastic strain.

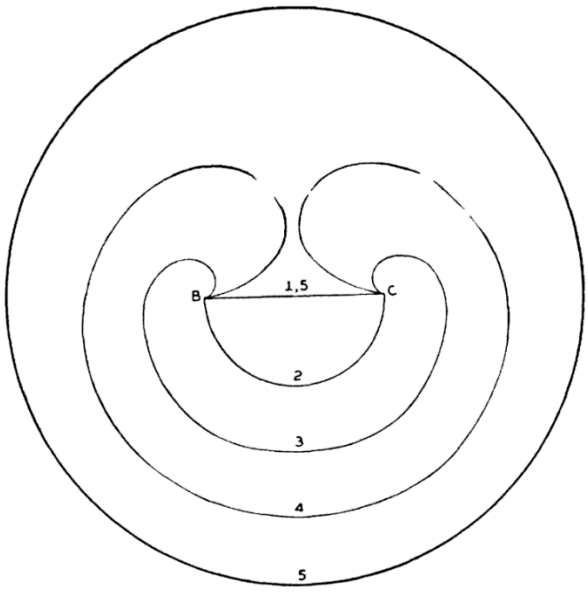

Figure 8: Generation of successive closed loops of dislocation line from a Frank-Read source [37].

The dislocations pileup at grain boundary can traverse the grain boundary or activate a new dislocation source in the neighboring grain so that neighboring grains will also undergo plastic strains. The dislocation pileup model is described mathematically by Hall-Petch equation [38],

$$\sigma_y = \sigma_0 + \frac{k_y}{\sqrt{d}},$$

where σ_y is the yield stress or flow stress, σ_0 is the resistance stress or back stress due to lattice friction, k_y is Petch parameter, also unknown as unpinning constant, d is the average grain diameter. Hall-Petch equation predicts that the yield stress is a function of grain size.

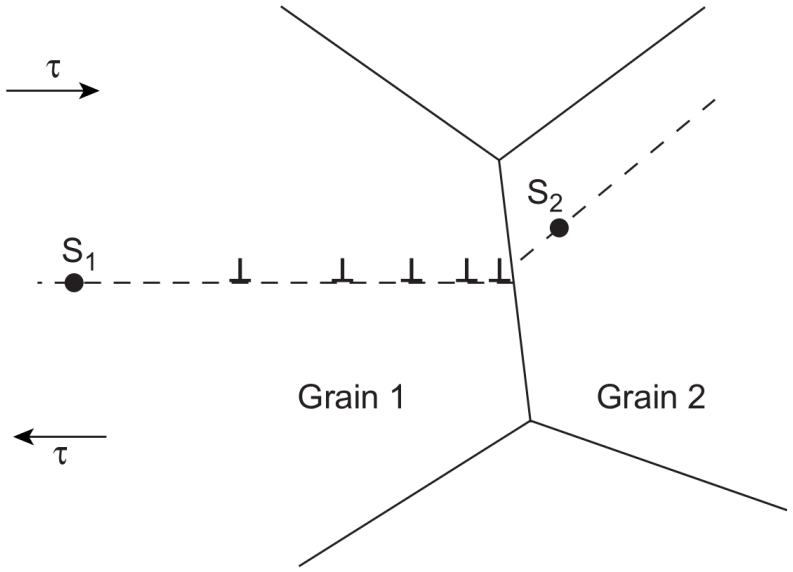

Figure 9: Schematics of piling-up of dislocations from the dislocation source S1 in grain 1 under a resolved shear stress τ. S2 is a dislocation source in grain 2. [39]

Predicted by Hall-Petch equation, the smaller grain size is, the larger the yield stress will be. With the Hall-Petch equation, the strengthening contribution which comes from grain size effects can be estimated. Hall-Petch equation remains valid until grain size decreases down to around 50 nm[40]. Smaller grain size leads to larger grain boundary density and smaller distance between two boundaries. When grain size reaches below 50 nm, grain size softening or reverse Hall-Petch effect will occur. The yield stress will decrease with the decrease of grain size. Many mechanisms like grain boundary sliding have been reported to explain this behavior [40]. With

such small grain size, dislocations are not allowed to pile up inside grains, which results in grain boundary sliding and grain rotation.

1.4.3 Solid Solution Strengthening

Magnesium is the principal solution element in 5083. The maximum solid solubility is 17.5% [32]. Besides magnesium, there are 0.7% manganese element and 0.15% chromium element as well. Solid solution atoms replace aluminum atoms in the Al matrix, forming point defects. Solid solution atoms act as barriers to dislocation slip. Upon deformation, dislocations can be pinned when they interaction with stationary solid solution elements. This pinning effect is one of the strengthening method caused by solid solution. What's more, other effects such as serrated flow and luder's band observed in the mechanical test are also related to interactions between solid solution atoms and dislocations. Serrated flow is known as the Portevin-Le Chatelier (PLC) effect, which is commonly observed in Al-Mg alloys [41,42]. PLC effect is classified into three types based on serration shape and strain rate[43]. Type A is found at a high strain rate. Type B is observed at a medium to high strain rate. Type C is observed at low strain rate. The mechanism accepted by most researchers is called dynamic strain aging (DSA) [44], which is described as interactions between dislocations and diffusive solid solution atoms.

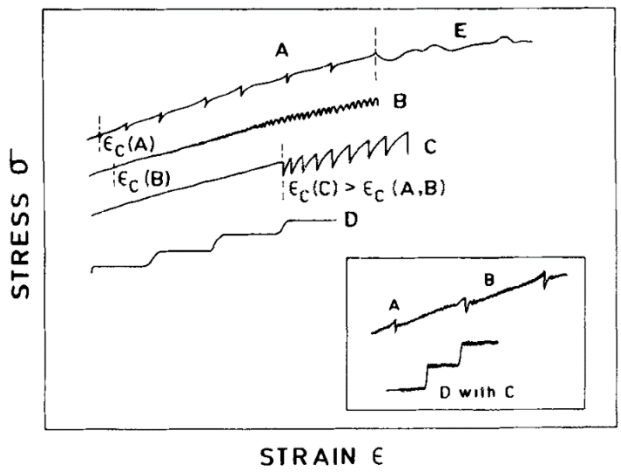

Figure 10: Different types of serrations in a stress-strain curve.

1.4.4 Precipitation Hardening

There are different kinds of magnesium precipitate in al-5083. It has been reported that Guinier-Preston (GP) zone first growthgrow from the supersaturated Mg solid solution which is often called α phase [45]. Precipitates are formed from GP zone with increasing annealing time at the different annealing temperature. GP zone gradually grows into β″ phase, β′ phase, and β phase [45]. The stoichiometric composition of GP zone in 5083 is Al_3Mg [3]. β″ phase is also known as ordered GP zone. It has the same stoichiometric composition with GP zone which is Al_3Mg [45]. Some researchers suggested that β″ possibly has an $L1_2$ structure [4]. β′ phase has a stoichiometric composition of Al_3Mg_2 and is a semi-coherent hexagonal intermediate phase which is reported to the main hardening phase in al-5083 [46]. The β phase is also known as Samson phase which is an equilibrium phase called with an FCC structure [46]. The stoichiometric composition of β phase is Al_3Mg_2. The formation of β phase at grain boundary will cause stress corrosion cracking because Al_3Mg_2 is anodic relative to Al matrix [47]. Mn-rich precipitates were also observed to be rod-like [47].

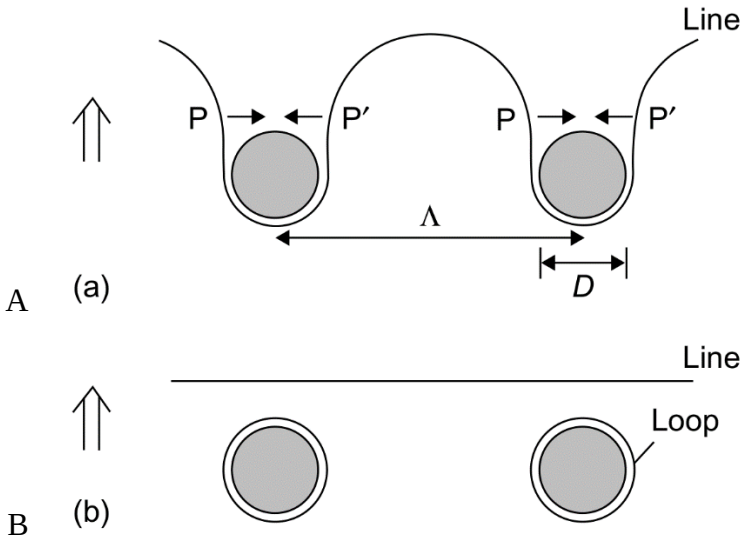

Figure 11: Schematics illustrating Orowan bypassing mechanism. (A) The dislocation line bows between two particles. (B) The line moves forward. [39]

Al-5083 is not classified as a precipitate hardening alloy. There are two types of well-found models describing dislocations – precipitates interactions, which are dislocation cutting through particles and dislocations bowing around particles. For coherent and semi-coherent precipitate particles, dislocations can cut through precipitate particles upon deformation because of the alignment between slip planes in precipitate particles and aluminum matrix. After cutting through by dislocations, particles will be sheared in the direction of dislocation moment. Cutting through effect is not as useful in semi-coherent particles as in coherent ones. Dislocations generated around the surface of semi-coherent particles will decrease volume misfit strain, making particle shearing less effective. For incoherent particles, slip planes are not aligned in particles and aluminum matrix. As a result, incoherent precipitate particles cannot be sheared by dislocations. When dislocations interact with incoherent particles, dislocations are likely to bypass these particles, ultimately forming dislocation loops. This mechanism is also called

Orowan bypassing or looping. The strengthening caused by Orowan looping. Orowan derived the very first equation describing dislocation bypassing a square distribution of particles [39],

$$\tau \approx \frac{\mu b}{l},$$

where τ is the shear stress, μ is the shear modulus, b is the magnitude of the burger vector, l is the average spacing between two neighboring particles. The strengthening effects contributed by precipitates can be estimated using this equation from Orowan bypassing mechanism.

1.5 Severe Cold Rolling of Aluminum and Aluminum Alloys

Several models have been proposed to explain grain refinement and the formation of subgrain structures in high SPE metals deformed by severe rolling at ambient temperature. Different models have been built to demonstrate the microstructural evolution by large strain deformation in polycrystalline materials for years, including Taylor's full constraint model which is best fit for describing homogeneous deformation in equiaxial grains [48]. According to Taylor's model, the uniform slip is achieved by activation of at least five slip systems in independent grains, however, deformation is not often uniform in real metals. Taylor's model has been modified by some researchers, but some details remain controversial. If the initial FCC metal is evenly deformed, initial coarse grains will be elongated [49]. Eventually, a ribbon grain structure will be formed by elongated grains separated by high angle grain boundaries. Within each grain, different slip systems are activated to accommodate plastic strain. When strain is further increased, dislocations are accumulated, forming dense dislocation walls (DDW) which divide grains into cell blocks [50]. Dislocation boundaries associated with cell blocks and smaller cells have been classified into two types: geometrically necessary boundaries and incidental dislocation boundaries [51,52]. Geometrically necessary boundaries are formed by

dislocations in different cell blocks interact with each other at the cell block boundaries. Geometrically necessary boundaries are generated to accommodate lattice rotation in the neighboring cell blocks. At an early stage of cold rolling, the misorientation of different cell blocks increases, gradually sub-dividing into new cells. To distinguish from cell blocks, new cells divided from cell blocks are call dislocation cells [51]. Dislocation cells in each cell block are separated by incidental dislocation boundaries. Incidental dislocation boundaries are formed by statistical mutual trapping of glide dislocations, often supplemented by "forest" dislocations [51]. The misorientation across geometrically necessary boundaries is larger than incidental dislocation boundaries [53]. As strain increases, cell blocks shrink faster than dislocation cells inside [51]. The number of dislocation cells per cell block decreases, ultimately decreases to one. The size of cell blocks decreases, however, misorientation increases. Some researchers proposed that geometrically necessary boundaries (GNBs) are formed between domains of different strain to accommodate the difference in lattice rotation and can become high angle boundaries under large strain; incidental dislocation boundaries (IDBs) are boundaries formed by random trapping of dislocations. [49,51,53]. Cell block walls belong to geometrically necessary boundaries; however, cell walls belong to incidental dislocation boundaries. Cells or subgrain structures are first formed inside grains at the early stage of deformation. These subgrain boundaries are incidental dislocation boundaries. At very large strain, the high angle boundaries tend to aligned in the rolling direction and the spacing between them will be reduced to the subgrain size [49].

2. Experimental Techniques and Methods

2.1 Experimental Procedures

A commercial Al-5083 alloy was studied in this research. Al-5083 alloy was received in plate form with a thickness of 10 mm. As-received commercial al-5083 alloy plates were first annealed at 500 °C for 5 h to reach a homogeneous supersaturate solid solution state. These Al-5083 plates were deformed by room temperature rolling with 10% thickness reduction each pass, until a total of 80% reduction in thickness was reached. No cracks were observed on the surface of these plates.

These as rolled Al-5083 plates were annealed under the temperature range from 200 °C to 300 °C with different annealing time from 5 mins to 20 mins in a tube furnace. Both as-rolled Al-5083 and as-annealed Al-5083 plates were polished into thin foils with a thickness less than 150 μm by mechanical polishing. These 5083 thin foils were then twin jet polished into TEM samples using a mixture solution of 75% methanol and 25% nitric acid at 243 K and potential of 25V. TEM images were taken by a JEOL 2000FX TEM under 200kV accelerating voltage. Mechanical properties, including uniaxial tensile tests and unloading-reloading tests, were measured by a Shimazu AGS universal testing machine. Samples used in uniaxial tensile tests were first machined from sheets processed by room temperature rolling, and then annealed at different conditions. Dog bone samples had a gauge dimension of $10\times2\times1.6$ mm^3.

2.2 Back stress measurement

Samples used in loading-unloading tests shared the same sample geometry with uniaxial tensile samples. Back stress calculations were done based on methods developed by M.Yang and co-workers in their previous work [33]. Back stress was calculated by

$$\sigma_b = \frac{\sigma_r + \sigma_u}{2},$$

where σ_b is the back stress, σ_r is the reloading yield stress, σ_u is the unloading yield stress. Two important assumptions were made in this work in order to derive the relationship between back stress, unloading yield stress, and reloading yield stress [33]. Firstly, the frictional stress stays constant in both unloading range and reloading range. Secondly, during unloading process, back stress is assumed to be constant before the unloading yield point.

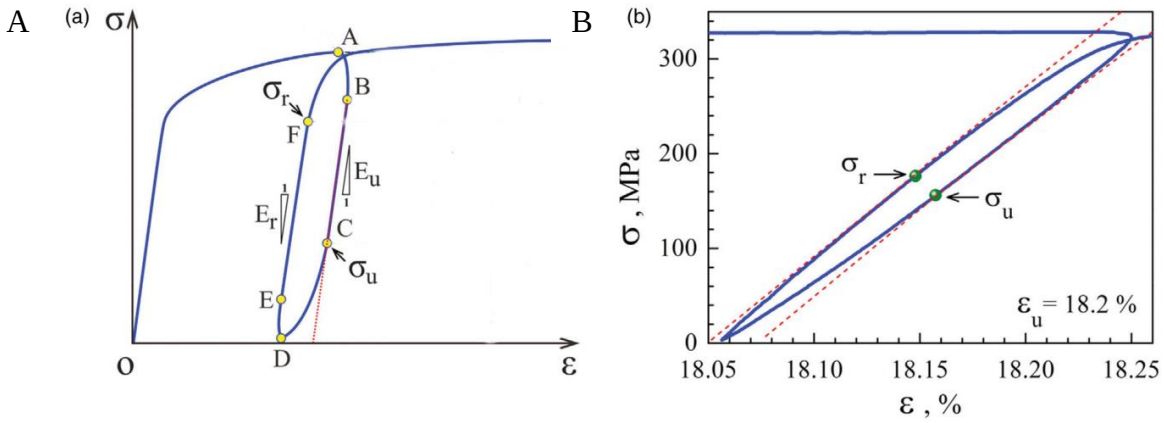

Figure 12: Schematics showing (A) an ideal unloading-reloading stress-strain curve, (B) a real unloading-reloading cycle.

The back stress equation was derived from the stress relations at both unloading yield point and reloading yield point. At unloading yield point, the back stress begins to overcome the

friction stress and the applied stress. Piled-up dislocations start to glide back, in the opposite direction of the applied stress. This leads to

$$\sigma_b = \sigma_u + \sigma_f,$$

where σ_f is the frictional stress. Similarly, at reloading yield point, dislocations start to pile up again, because the applied stress starts to overcome the back stress and the friction stress, which is

$$\sigma_r = \sigma_b + \sigma_f.$$

Taken the two assumptions, the back stress can be calculated from the unloading yield stress and the reloading yield stress.

3. Experimental Results

3.1 Microstructure Characterization of Heterogeneous-Structured Al-5083

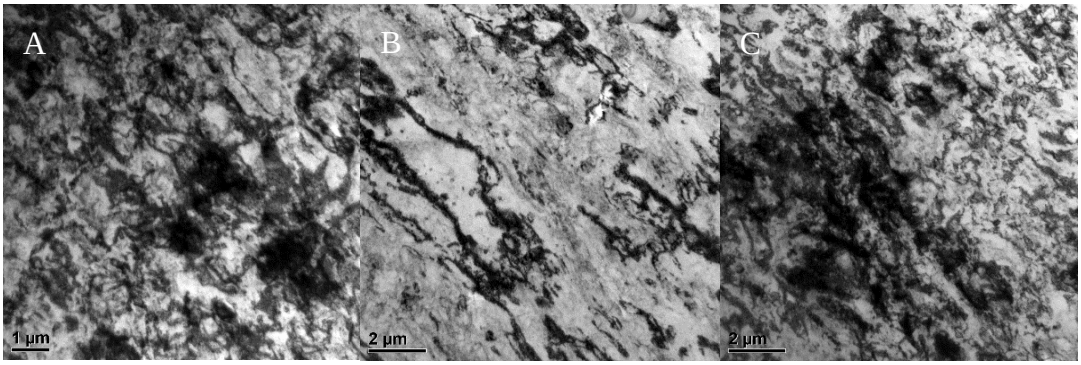

Figure 13 TEM images of (A) equaxial grains; (B) elongated grains and isolated subgrains; (C)cell blocks and dislocation tangled zones in al-5083 with 80% rolling reduction

As-received commercial al-5083 alloy plates were first annealed at 500 °C for 5 h to reach a homogeneous supersaturate solid solution state. Then, al-5083 plates were rolled at room temperature until 80% thickness reduction was reached. Fig 13(A), (B) and (C) are TEM images of as-rolled Al-5083 plates. The grain size ranges from 1μm to a few micrometers. Subgrain structures are also observed with size smaller than 1 μm. After rolling with 80% thickness reduction, initial coarse grain samples were severely deformed, generating dislocation-tangle zones well spread across the sample. Fig 13(A) shows large density of dislocation walls and dislocation tangled zones. Small grains separated by dense dislocation walls are possibly evolved from cell blocks. Within these grains, subgrain structures are observed, which are possibly originated from dislocation cells inside cell blocks. In each newly formed fine grain (around a few microns), the number of subgrains per grain ranges from 2 to 3. Three kinds of dislocation walls are observed, which are dense dislocation walls [50], uncondensed dislocation walls [54], and clustered-small-cell walls [53]. Clustered-small-cell walls are consisted of equiaxed, sub-

divided dislocation cells [53]. In fig 13(B), an elongated grain longer than 8 μm is observed, surrounded by uncondensed dislocation walls and clustered-small-cell-wall [53]. Isolated subgrains are observed near the boundary of the elongated grain. These subgrains have sizes smaller than 1 μm. Intensities from most areas differ slightly, indicating small misorientation across the area. Fig 13(C) shows a large area of dislocation-tangle zones accompanied by cell blocks and clustered-small-cell walls. Dislocation-tangle zones appear as continuous dark areas in TEM images.

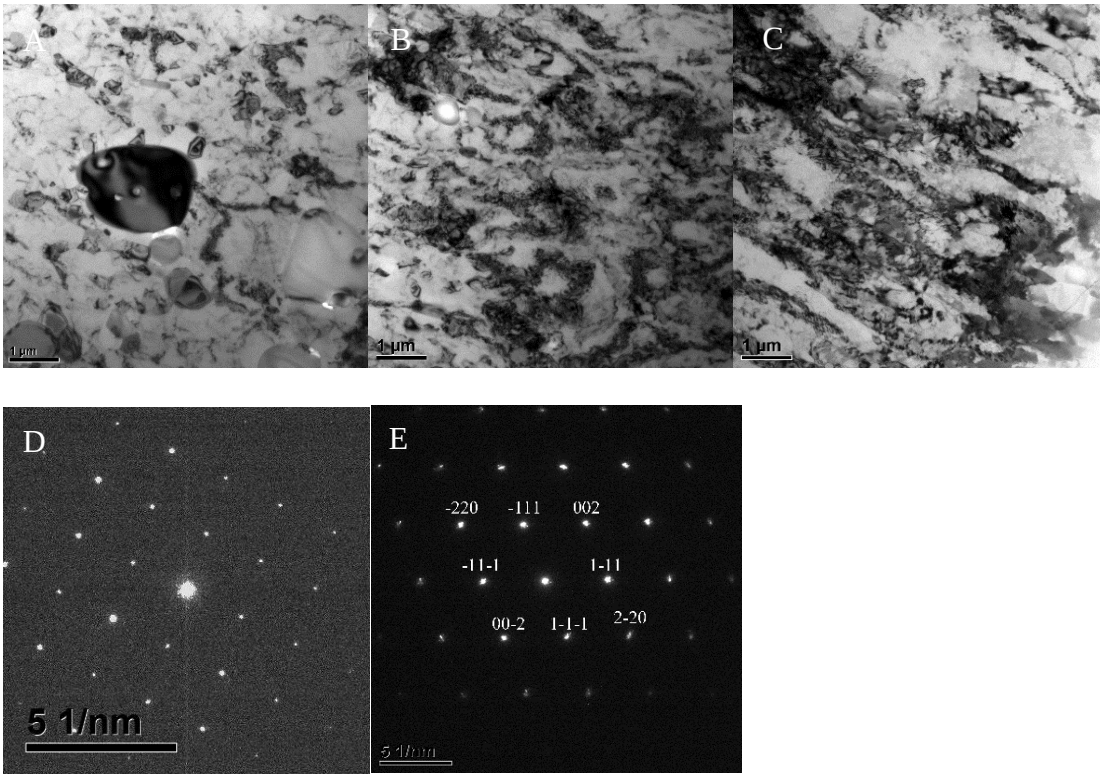

Figure 14: TEM images of (A) oval shape precipitates; (B) subgrain structures (C) elongated grains; and diffraction pattern of (D) oval shape precipitates (E) al-5083 matrix in 80% rolled 5083 with annealing at 230°C for 10 mins.

After annealing at 230 ℃ for 10 mins, precipitations are observed. From the literature, precipitation sequence in an Al-Mg alloy is usually as supersaturated solid solution α phase – GP zone - β″ phase - β′ phase - β phase [45]. Guinier–Preston Zones (GP zones) has a stochiometric composition of Al_3Mg, which is short-range ordered. β″ phase possibly has an $L1_2$ structure, and its composition is suggested to be Al_3Mg[47]. β′ phase is a semi-coherent hexagonal intermediate phase with a composition of Al_3Mg_2 (a=1.002 nm, c=1.636 nm)[46]. The β phase is an equilibrium phase called Samson phase and is of an FCC structure with the composition of Al_3Mg_2 [47]. Fig 14(A) shows oral-shaped precipitates and rod-like precipitates. The oral-shaped precipitate is almost 2 μm and overlapped on the al-5083 matrix in the TEM image. Selected area electron diffraction (SAED) pattern indicates that the oral-shaped precipitate is the closest to the intermediate β′ phase [211] zone axis. The rod-like precipitation is possibly to be an Mn-rich precipitate [47]. Fringes around the oval-shaped precipitation could be some other kinds of precipitations. Precipitates are not evenly spread throughout the as-annealed samples. Precipitate-free areas are also observed. Fig 14(D) shows that a large area of subgrain structure and subdivided clustered-small-cell walls remain in al-5083 samples after annealing for 10 mins under 230°C. The SAED take from the surrounding matrix is corresponding to [110] zone axis in FCC. Fig 14(E) shows ribbon-like structure consisted of elongated grains with subgrains inside. Subgrain structure and elongated grains remain after annealing.

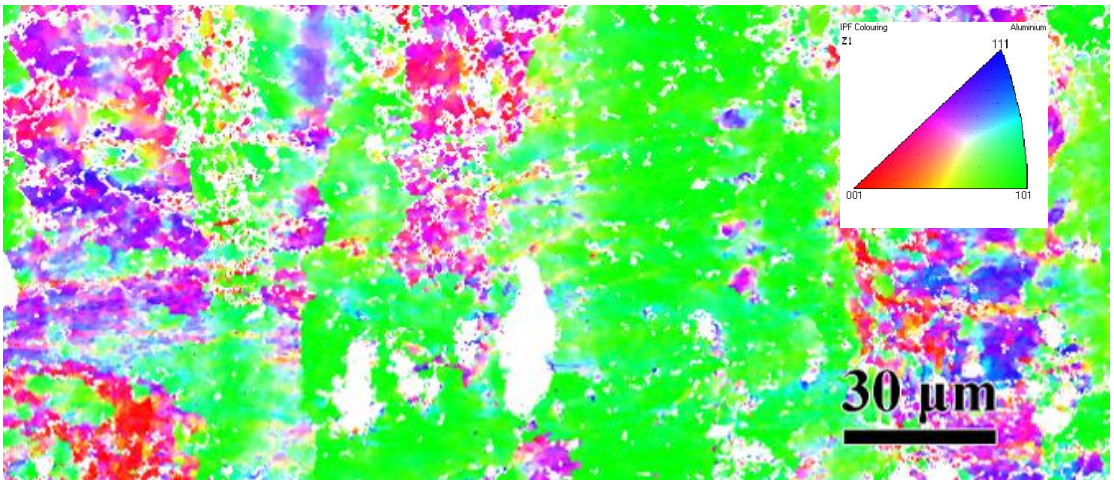

Figure 15: EBSD image of 80% rolled 5083 samples with annealing at 230°C for 10 mins.

Two kinds of domains are clearly shown in the EBSD picture. Large domains consist of grains in [101] orientation, separated by domains of fine grains. In previous studies, large domains in the same orientation are considered as soft domains. The soft domains are possibly originated from the same grain after rolling and annealing. The misorientation between them is so small that they all appear in the same color in the EBSD image. Surrounding areas consisted of fine grains are considered as hard domains. The hard domain consists of small grains in different orientations. The thickness of the hard domains measured from the EBSD image is ranging from 25 to 40 µm. The distance between two different hard domains is around 70 to 75 µm. Hard domains with orientations other than [101] are embedded in a large area of soft domains.

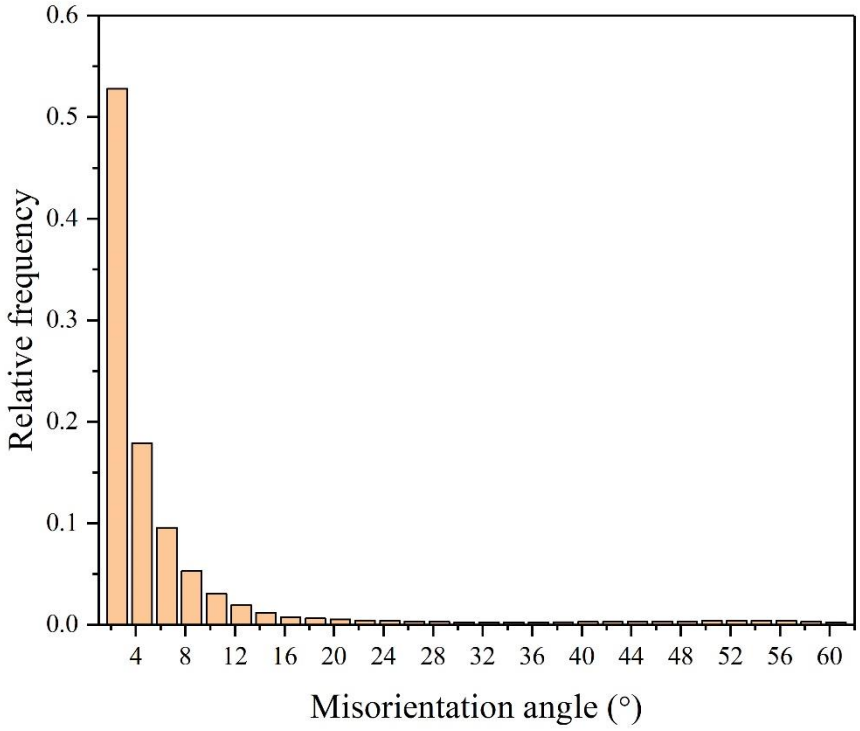

Figure 16: Misorientation angles of 80% rolled 5083 samples with annealing at 230°C for 10 mins.

Within all correlated misorientation angles, around 45% misorientation angles are smaller than 15°, which are generally considered to be separated by low angle boundaries. Less than 1 percent misorientation angles are larger than 15°, which are separated by high angle boundaries. Around 35% misorientation angles are smaller than 5°.

Table 2: Grain size distribution of as-rolled al-5083

with different annealing parameters.

	Grain size distribution				
Annealing	1-10 (μm)	10-20 (μm)	20-30 (μm)	30-40 (μm)	40-50 (μm)
230°C5M	417	20	4	0	0
230°C10M	1756	16	3	0	1

For as-rolled al-5083 samples, the grain size is estimated via an optical microscope and TEM. Most grains are around 1-2 μm, however, a few large grains with a size around 8 μm are also observed. The density of precipitations is hard to estimate via either TEM or optical microscope. Under an optical microscope, a large area can be explored, but precipitations are hard to be distinguished from its matrix by etching. Grain size information is further gathered by EBSD data. Limited by scanning step size, grain size less than 1 μm cannot be recognized in the EBSD image for 5 min annealing samples. Most grains range from 1 to 10 μm. No grain larger than 30 μm was observed. For 10 min annealing samples, most grains are still less than 10 μm. On the other hand, a grain was observed to be larger than 40 μm.

3.2 Mechanical Properties of Heterogenous-structured Al-5083

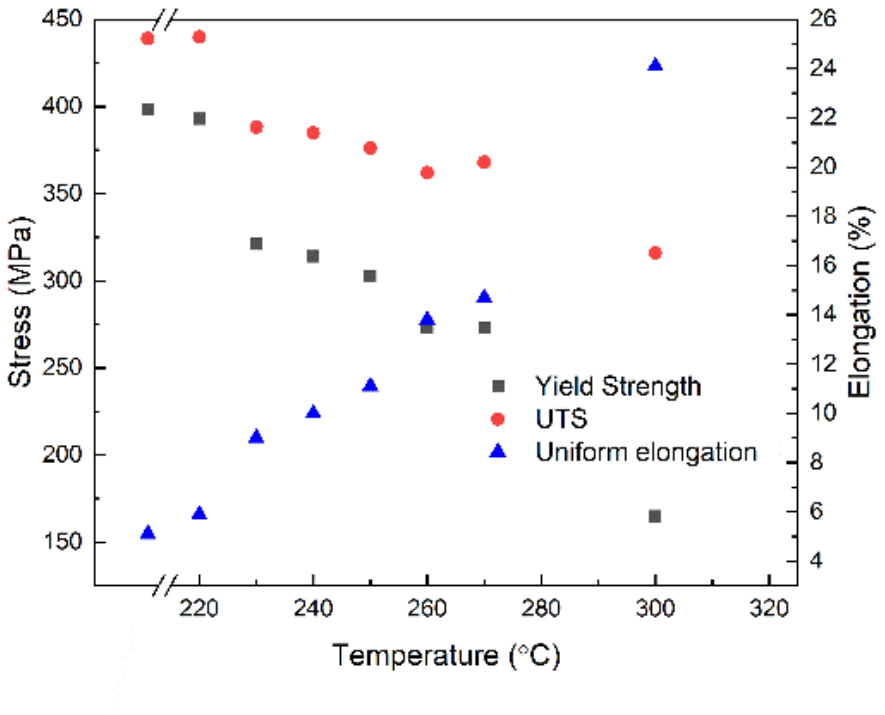

Figure 17: The effects of annealing temperature on al-5083 alloy with 80% thickness reduction and annealed for 5 mins.

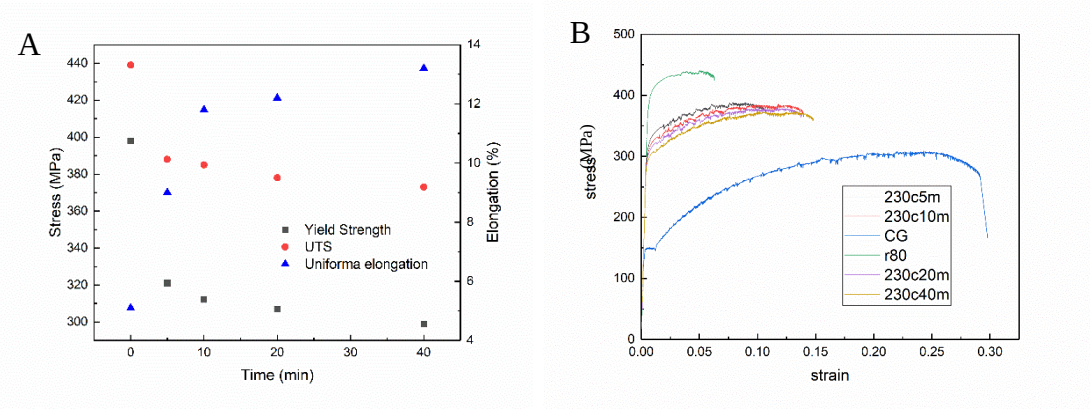

Figure 18: (A) The effects of annealing time; (B) tensile stress-strain curve of al-5083 alloy with 80% thickness reduction and annealed at 230°C.

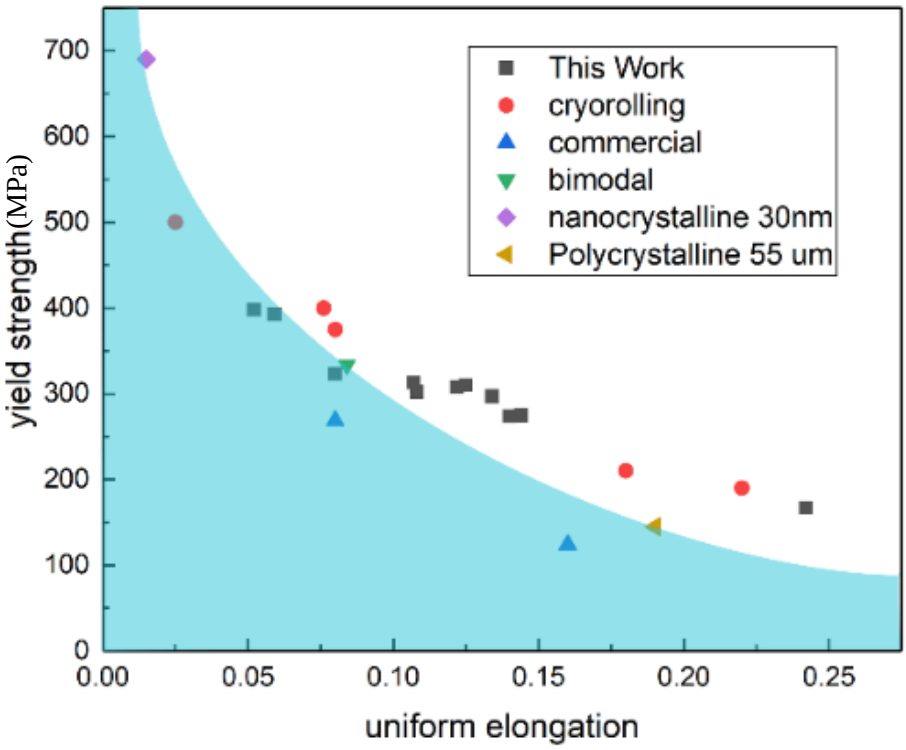

Figure 18: Yield strength and uniform elongation al-5083 in this work and other data for comparison.

Fig. 17 and 18 shows the result of the uniaxial tensile test results for different samples. Each condition is tested 4 times for accuracy. To investigate the effects of partial recrystallization on mechanical properties, as-rolled al-5083 samples were annealed under different temperature for 5 mins. Results were summarized in fig. 17. The leftmost data belongs to as-rolled al-5083 with 80% thickness reduction for comparison. Upper yield point and lower point were observed in curves taken from 300 ℃ samples and coarse grain samples. Annealed at 220 ℃， the uniaxial tensile properties stay almost the same. From 200 ℃ to 230 ℃, both yield strength and ultimate yield strength drop dramatically by 19%, however, uniform elongation increases by 76%. Before 300℃, yield strength gradually dropped with an increase of annealing temperature and the rate of decrease gradually increased. Beyond 300℃, the drop started to slowdown. There was 3% difference in yield strength and 4% difference in uniform elongation between 300 ℃ samples and homogeneous coarse grain samples (500 ℃ 5h). The ultimate stress reached a plateau between 230 ℃ and 270 ℃. Based on a combination of yield strength and uniform elongation, 230 ℃ was selected for further investigation on partial recrystallization time influence. As shown in fig 18(A) and 18(B), the yield stress dropped 80 MPa upon annealing, then dropped slowly with the increase of time. The uniform elongation increased significantly until annealing time reached 10 mins. In all the samples tested, zig-zag curves were observed, which was corresponding to Portevin–Le Chatelier (PLC) band.

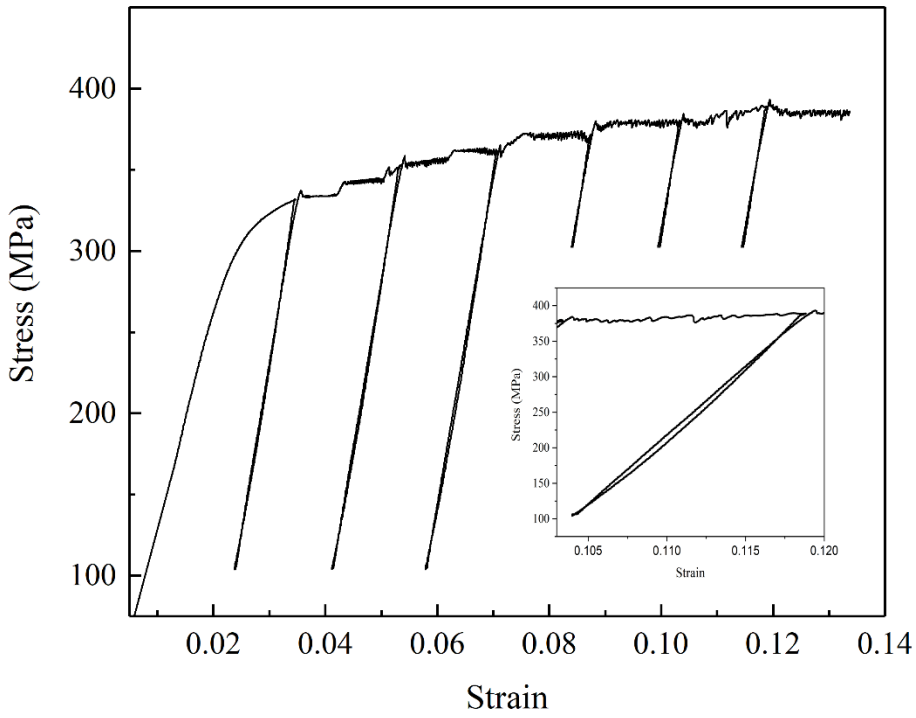

Figure 19: Unloading-reloading stress-strain curve of as-rolled samples with 230°C 10min annealing.

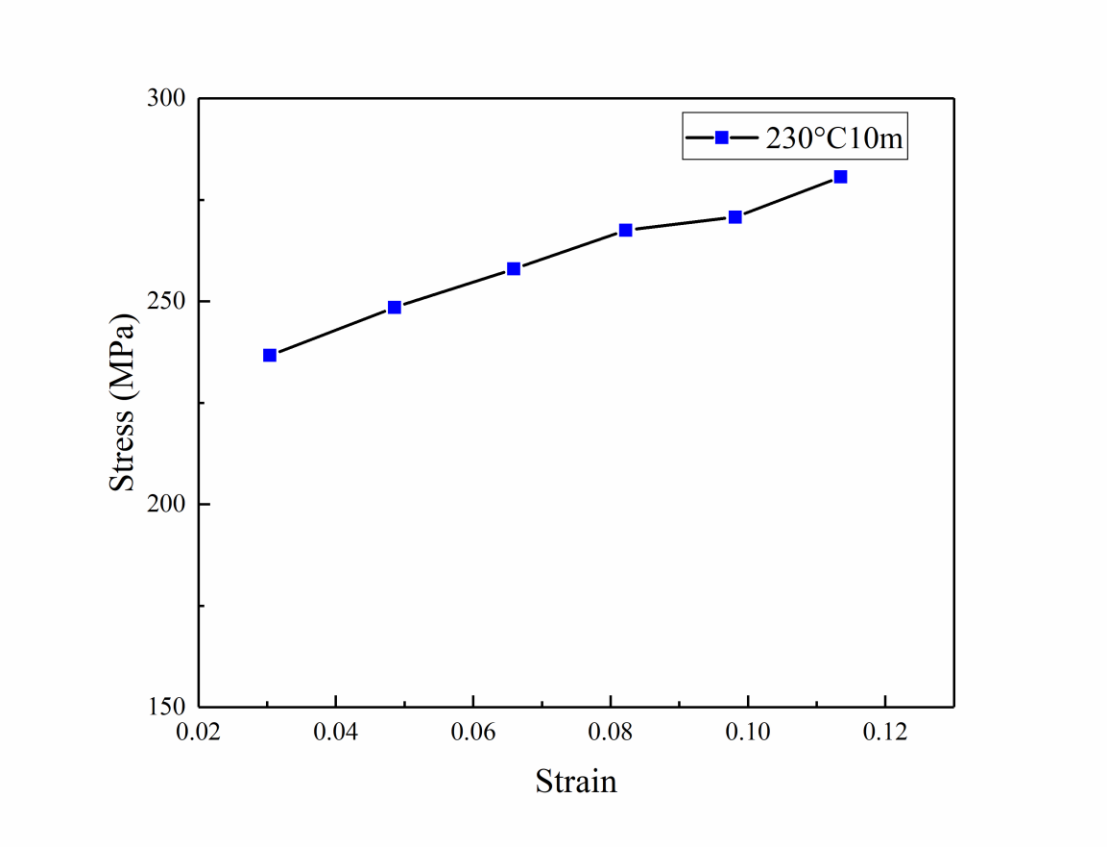

Figure 20: Back stress versus applied strain of as-rolled samples with 230°C 10min annealing.

Table 3: Back stress of annealed al-5083 and coarse grain samples.

	R80+230°C 10M	Coarse grain
Back stress (MPa)	271	121

Back stress measurement was performed at 230 °C 10 mins samples and 500°C 5 h (coarse grain) samples. In 230 °C 10 mins samples, the back stress measured was almost 150 MPa higher than the coarse grain ones.

4. Discussion

4.1 Microstructures evolution

Detailed microstructural features are investigated by TEM. Observed from TEM images in fig.13, the grain size of as-rolled samples is in the range of 1 to 10 μm. Most equiaxed grains range from 1 to 2 μm. Elongated grains are observed to be 8 μm long and 2 μm wide. Isolated subgrains are observed in the elongated grains. Rolling was performed with 10% thickness reduction per pass, until a total of 80% reduction was reached. A modified Taylor's model was the best approach to describe microstructure evolution during severe rolling at ambient temperature [48]. At the early stage of rolling, slip systems were activated in each coarse grain to accommodate the plastic strain introduced by shear forces. Dislocation walls and dislocation tangled zones started to form, which divided grains into volume elements called cell blocks. With increasing strain, the misorientation angles between different cell blocks increased. Eventually, new grains formed at the place of cell blocks. Al-5083 plates were not deformed homogeneously by cold rolling at ambient temperature. Elongated grains and equiaxial grains were observed in as-rolled samples and annealed samples.

After partial recrystallization, two kinds of different domains were formed in EBSD images, soft domains and hard domains. The alternate arrangement of hard domains and soft domains formed a heterogeneous lamellar structure in annealed al-5803 samples.

One domain consisted of grains with mainly [101] orientation and tiny deviation, which would behave as a soft domain. This large soft domain was possibly recrystallized from one original grain with subgrain structures. Because of the uniform deformation by room temperature rolling, subgrains and cell blocks did not further deformed into plate-like, severely elongated grains which were dominant in severe rolling aluminum [49]. As shown in fig 13(A) and 13(C),

subgrain structure partly remained in equiaxed cells and dislocation tangled zones while others were severely elongated into the plate-like structure. As shown in fig. 14(C), plate-like structure remained after annealing at 230°C for 10 minutes.

Another domain consisted of small grains in many different orientations. The domain of large grains offered larger dislocation pile-up ability than the adjacent domains of small grains. At the early stage of deformation, large grains would start to deform first. Until the strain in large grains reached a critical value, domains of small grains would start to deform. In this way, the large grains areas were considered as soft domains. On the contrary, small grains areas were considered as hard domains. The continuous hard domain would act as a constraint to the deformation of soft domains.

4.2 Strengthening Mechanisms and Back Stress Strengthening in Al-5083

Al-5083 samples presented in this research (80% thickness reduction and annealing) were as good as cryo-rolling 5083 (85% reduction and annealing) in mechanical properties [55]. Summarized in fig 16(B), cryo-rolling 5083 exhibited higher yield stress (522 MPa) than room temperature rolling with similar thickness reduction, however, mechanical properties were almost the same after annealing. It was the result of heterogeneous lamella structure in our 5083 samples. During cryo-rolling, dynamic recovery was suppressed by the low temperature, eventually achieving smaller average grain size and high density of dislocations than room temperature rolling [55]. Predicted by some of the earlier models on large strain deformation [49], initial grains were deformed into severely elongated grains (400 – 800 nm in length and 50 – 100 nm in width) under very large strain, forming a plate-like structure [55]. In our work, severely elongated grains only made up a small percentage after room temperature rolling.

Strengthening mechanisms which are possibly involved in al-5083 are back stress strengthening, solute strengthening, precipitate strengthening, grain boundary strengthening, and dislocation wall strengthening. The contribution from each mechanism will be discussed according.

Back stress is primary responsible for the improvement of yield stress and ductility. Annealed at 230°C from 5 mins to 10 mins, yield stress decreased 2.8%, which was 9 MPa, however, uniform elongation increased from 9% to 12%. Average grain sizes were almost the same, except few grains were found larger than 40 μm in 10 mins samples. The back stress of 10 mins annealed samples was 175 MPa larger than the coarse grain ones. The sample consisted of soft domains and hard domains, which laid next to each other in a lamellar shape. Two hard domains were separated by a soft domain with grains in [101] orientation. The average distance between two hard domains was around 70 μm. Upon deformation, the soft domain would undergo plastic deform before the hard counterparts started to deform. The strain in soft domains was much larger than in hard domians. The strain partition caused geometrically necessary dislocations to pile up at the interface on the soft domain side, which generated back stress, which was in the opposite direction to the applied stress. The effective stress equaled to the difference between applied stress and back stress. Effective stress needed to surplus a critical value so that more dislocation would be operated and pile up. As a result, a larger applied stress would be needed to pile up more and more dislocations.

Grain boundary strengthening and dislocation forest played other important roles, however, ductility is the cost of the strengthening. Yield stress was increased from 150 MPa to 398 MPa when grain size was refined from initial homogeneous coarse grains to 1 μm by cold rolling. Ductility was reduced from 24.9% to 5.1%. Grain boundary and dislocation forest were two

great barriers to dislocation motion. With larger areas of grain boundaries and larger density of dislocation forest, more dislocation could be stored during deformation.

Solute strengthening and precipitate strengthening show little difference between different samples. There was no difference in composition elements between each sample. The principal solution elements in Al-5083 samples are magnesium and manganese. Precipitates were found Under TEM, for example, Al-Mg β' phase precipitates which were reported to be a hardening phase in Al-Mg alloys. Precipitate strengthening mechanism could be explained by Orowan looping,

$$\tau \approx \frac{\mu b}{l}.$$

The shear force was inversely proportional to the distance between two closest precipitates. In 10 mins annealed al-5003 samples, precipitates were not widespread across the samples. Average distance was around a few microns. In this case, the precipitate strengthening effect was too small compared with back stress strengthening.

5. Conclusion

1. In this work, a heterogenous lamella structure was reported in aluminum alloy 5083 for the first time.
2. Reported al-5083 samples showed mechanical properties as good as cryo-rolling and annealing 5083 samples. Our process is more environmentally friendly and economical for mass production.
3. Microstructure evolution was examined by TEM and EBSD, confirming the formation of a heterogeneous lamella structure.
4. Different strengthening mechanisms in al-5083 were evaluated. Back stress strengthening was the dominant strengthening mechanism in our 5083 samples.

REFERENCES

[1] D. Gay, S.V. Hoa, S.W. Tsai, Composite materials design and applications, CRC Press, Boca Raton, FL, 2003.

[2] Y.T. Zhu, X. Liao, Retaining ductility: Nanostructured metals, Nat. Mater. 3 (2004) 351–352. doi:10.1038/nmat1141.

[3] Y.-H. Zhao, J.F. Bingert, X.-Z. Liao, B.-Z. Cui, K. Han, A.V. Sergueeva, A.K. Mukherjee, R.Z. Valiev, T.G. Langdon, Y.T. Zhu, Simultaneously Increasing the Ductility and Strength of Ultra-Fine-Grained Pure Copper, Adv. Mater. 18 (2006) 2949–2953. doi:10.1002/adma.200601472.

[4] Y. Zhao, Y. Zhu, E.J. Lavernia, Strategies for Improving Tensile Ductility of Bulk Nanostructured Materials, Adv. Eng. Mater. 12 (2010) 769–778. doi:10.1002/adem.200900335.

[5] Y.H. Zhao, X.Z. Liao, Z. Horita, T.G. Langdon, Y.T. Zhu, Determining the optimal stacking fault energy for achieving high ductility in ultrafine-grained Cu–Zn alloys, Mater. Sci. Eng. A. 493 (2008) 123–129. doi:10.1016/j.msea.2007.11.074.

[6] X. Wu, Y. Zhu, Heterogeneous materials: a new class of materials with unprecedented mechanical properties, Mater. Res. Lett. 5 (2017) 527–532. doi:10.1080/21663831.2017.1343208.

[7] K. Lu, J. Lu, Nanostructured surface layer on metallic materials induced by surface mechanical attrition treatment, Mater. Sci. Eng. A. 375–377 (2004) 38–45. doi:10.1016/j.msea.2003.10.261.

[8] K. Lu, Making strong nanomaterials ductile with gradients, Science. 345 (2014) 1455–1456. doi:10.1126/science.1255940.

[9] X.L. Wu, M.X. Yang, F.P. Yuan, L. Chen, Y.T. Zhu, Combining gradient structure and TRIP effect to produce austenite stainless steel with high strength and ductility, Acta Mater. 112 (2016) 337–346. doi:10.1016/j.actamat.2016.04.045.

[10] Y. Wang, M. Chen, F. Zhou, E. Ma, High tensile ductility in a nanostructured metal, 419 (2002) 4.

[11] B.O. Han, E.J. Lavernia, Z. Lee, S. Nutt, D. Witkin, Deformation behavior of bimodal nanostructured 5083 Al alloys, Metall. Mater. Trans. A. 36 (2005) 957–965. doi:10.1007/s11661-005-0289-7.

[12] C.X. Huang, Y.F. Wang, X.L. Ma, S. Yin, H.W. Höppel, M. Göken, X.L. Wu, H.J. Gao, Y.T. Zhu, Interface affected zone for optimal strength and ductility in heterogeneous laminate, Mater. Today. (2018). doi:10.1016/j.mattod.2018.03.006.

[13] X. Ma, C. Huang, J. Moering, M. Ruppert, H.W. Höppel, M. Göken, J. Narayan, Y. Zhu, Mechanical properties of copper/bronze laminates: Role of interfaces, Acta Mater. 116 (2016) 43–52. doi:10.1016/j.actamat.2016.06.023.

[14] X.L. Ma, C.X. Huang, W.Z. Xu, H. Zhou, X.L. Wu, Y.T. Zhu, Strain hardening and ductility in a coarse-grain/nanostructure laminate material, Scr. Mater. 103 (2015) 57–60. doi:10.1016/j.scriptamat.2015.03.006.

[15] C. Sawangrat, S. Kato, D. Orlov, K. Ameyama, Harmonic-structured copper: performance and proof of fabrication concept based on severe plastic deformation of powders, J. Mater. Sci. 49 (2014) 6579–6585. doi:10.1007/s10853-014-8258-4.

[16] S.K. Vajpai, M. Ota, T. Watanabe, R. Maeda, T. Sekiguchi, T. Kusaka, K. Ameyama, The Development of High Performance Ti-6Al-4V Alloy via a Unique Microstructural Design with Bimodal Grain Size Distribution, Metall. Mater. Trans. A. 46 (2015) 903–914.

doi:10.1007/s11661-014-2649-7.

[17] X. Wu, F. Yuan, M. Yang, P. Jiang, C. Zhang, L. Chen, Y. Wei, E. Ma, Nanodomained Nickel Unite Nanocrystal Strength with Coarse-Grain Ductility, Sci. Rep. 5 (2015). doi:10.1038/srep11728.

[18] M. Calcagnotto, Y. Adachi, D. Ponge, D. Raabe, Deformation and fracture mechanisms in fine- and ultrafine-grained ferrite/martensite dual-phase steels and the effect of aging, Acta Mater. 59 (2011) 658–670. doi:10.1016/j.actamat.2010.10.002.

[19] Z. Li, K.G. Pradeep, Y. Deng, D. Raabe, C.C. Tasan, Metastable high-entropy dual-phase alloys overcome the strength–ductility trade-off, Nature. 534 (2016) 227–230. doi:10.1038/nature17981.

[20] K. Lu, F.K. Yan, H.T. Wang, N.R. Tao, Strengthening austenitic steels by using nanotwinned austenitic grains, Scr. Mater. 66 (2012) 878–883. doi:10.1016/j.scriptamat.2011.12.044.

[21] L. Lu, X. Chen, X. Huang, K. Lu, Revealing the Maximum Strength in Nanotwinned Copper, Science. 323 (2009) 607–610. doi:10.1126/science.1167641.

[22] X. Wu, M. Yang, F. Yuan, G. Wu, Y. Wei, X. Huang, Y. Zhu, Heterogeneous lamella structure unites ultrafine-grain strength with coarse-grain ductility, Proc. Natl. Acad. Sci. 112 (2015) 14501–14505. doi:10.1073/pnas.1517193112.

[23] X. Wu, P. Jiang, L. Chen, F. Yuan, Y.T. Zhu, Extraordinary strain hardening by gradient structure, Proc. Natl. Acad. Sci. 111 (2014) 7197–7201. doi:10.1073/pnas.1324069111.

[24]Z. Ma, J. Liu, G. Wang, H. Wang, Y. Wei, H. Gao, Strength gradient enhances fatigue resistance of steels, Sci. Rep. 6 (2016). doi:10.1038/srep22156.

[25] J. Moering, X. Ma, J. Malkin, M. Yang, Y. Zhu, S. Mathaudhu, Synergetic strengthening far beyond rule of mixtures in gradient structured aluminum rod, Scr. Mater. 122 (2016) 106–

109. doi:10.1016/j.scriptamat.2016.05.006.

[26] Y.S. Zhang, Z. Han, K. Wang, K. Lu, Friction and wear behaviors of nanocrystalline surface layer of pure copper, Wear. 260 (2006) 942–948. doi:10.1016/j.wear.2005.06.010.

[27] X.L. Wu, P. Jiang, L. Chen, J.F. Zhang, F.P. Yuan, Y.T. Zhu, Synergetic Strengthening by Gradient Structure, Mater. Res. Lett. 2 (2014) 185–191. doi:10.1080/21663831.2014.935821.

[28] L. Zhu, S. Shi, K. Lu, J. Lu, A statistical model for predicting the mechanical properties of nanostructured metals with bimodal grain size distribution, Acta Mater. 60 (2012) 5762–5772. doi:10.1016/j.actamat.2012.06.059.

[29] Z. Zhang, S.K. Vajpai, D. Orlov, K. Ameyama, Improvement of mechanical properties in SUS304L steel through the control of bimodal microstructure characteristics, Mater. Sci. Eng. A. 598 (2014) 106–113. doi:10.1016/j.msea.2014.01.023.

[30] T. Sekiguchi, K. Ono, H. Fujiwara, K. Ameyama, New Microstructure Design for Commercially Pure Titanium with Outstanding Mechanical Properties by Mechanical Milling and Hot Roll Sintering, Mater. Trans. 51 (2010) 39–45. doi:10.2320/matertrans.MB200913.

[31] H. Fujiwara, T. Kawabata, H. Miyamoto, K. Ameyama, Mechanical Properties of Harmonic Structured Composite with Pure Titanium and Ti–48 at%Al Alloy by MM/SPS Process, Mater. Trans. 54 (2013) 1619–1623. doi:10.2320/matertrans.MH201317.

[32] J.R. Davis, ed., Alloying: understanding the basics, ASM International, Materials Park, OH, 2001.

[33] M. Yang, Y. Pan, F. Yuan, Y. Zhu, X. Wu, Back stress strengthening and strain hardening in gradient structure, Mater. Res. Lett. 4 (2016) 145–151. doi:10.1080/21663831.2016.1153004.

[34] H. Gao, Y. Huang, Geometrically necessary dislocation and size-dependent plasticity, Scr. Mater. 48 (2003) 113–118. doi:10.1016/S1359-6462(02)00329-9.

[35] H. Gao, Mechanism-based strain gradient plasticity? I. Theory, J. Mech. Phys. Solids. 47 (1999) 1239–1263. doi:10.1016/S0022-5096(98)00103-3.

[36] L.E. Murr, Dislocation Ledge Sources: Dispelling the Myth of Frank–Read Source Importance, Metall. Mater. Trans. A. 47 (2016) 5811–5826. doi:10.1007/s11661-015-3286-5.

[37] F.C. Frank, W.T. Read, Multiplication Processes for Slow Moving Dislocations, Phys. Rev. 79 (1950) 722–723. doi:10.1103/PhysRev.79.722.

[38] N. Hansen, Hall–Petch relation and boundary strengthening, Scr. Mater. 51 (2004) 801–806. doi:10.1016/j.scriptamat.2004.06.002.

[39] D. Hull, D.J. Bacon, Introduction to dislocations, 5. ed, Elsevier/Butterworth-Heinemann, Amsterdam, 2011.

[40] H. Conrad, J. Narayan, On the grain size softening in nanocrystalline materials, Scr. Mater. 42 (2000) 1025–1030. doi:10.1016/S1359-6462(00)00320-1.

[41] H. Halim, D. Wilkinson, M. Niewczas, The Portevin–Le Chatelier (PLC) effect and shear band formation in an AA5754 alloy, Acta Mater. 55 (2007) 4151–4160. doi:10.1016/j.actamat.2007.03.007.

[42] A.H. Cottrell, LXXXVI. A note on the Portevin-Le Chatelier effect, Lond. Edinb. Dublin Philos. Mag. J. Sci. 44 (1953) 829–832. doi:10.1080/14786440808520347.

[43]P. Rodriguez, Serrated plastic flow, Bull. Mater. Sci. 6 (1984) 653–663. doi:10.1007/BF02743993.

[44] A. van den Beukel, Theory of the effect of dynamic strain aging on mechanical properties, Phys. Status Solidi A. 30 (1975) 197–206. doi:10.1002/pssa.2210300120.

[45] K. Osamura, T. Ogura, Metastable phases in the early stage of precipitation in Al-Mg alloys, Metall. Trans. A. 15 (1984) 835–842. doi:10.1007/BF02644557.

[46] J. Yan, A.M. Hodge, Study of β precipitation and layer structure formation in Al 5083: The role of dispersoids and grain boundaries, J. Alloys Compd. 703 (2017) 242–250. doi:10.1016/j.jallcom.2017.01.360.

[47] R. Goswami, G. Spanos, P.S. Pao, R.L. Holtz, Precipitation behavior of the ß phase in Al-5083, Mater. Sci. Eng. A. 527 (2010) 1089–1095. doi:10.1016/j.msea.2009.10.007.

[48] H.-R. Wenk, P.V. Houtte, Texture and anisotropy, Rep. Prog. Phys. 67 (2004) 1367–1428. doi:10.1088/0034-4885/67/8/R02.

[49] F.J. Humphreys, P.B. Prangnell, J.R. Bowen, A. Gholinia, C. Harris, Developing stable fine-grain microstructures by large strain deformation, Philos. Trans. R. Soc. Math. Phys. Eng. Sci. 357 (1999) 1663–1681. doi:10.1098/rsta.1999.0395.

[50] B. Bay, N. Hansen, D.A. Hughes, D. Kuhlmann-Wilsdorf, Overview no. 96 evolution of f.c.c. deformation structures in polyslip, Acta Metall. Mater. 40 (1992) 205–219. doi:10.1016/0956-7151(92)90296-Q.

[51] D. Kuhlmann-Wilsdorf, N. Hansen, Geometrically necessary, incidental and subgrain boundaries, Scr. Metall. Mater. 25 (1991) 1557–1562. doi:10.1016/0956-716X(91)90451-6.

[52] D.. Hughes, N. Hansen, D.. Bammann, Geometrically necessary boundaries, incidental dislocation boundaries and geometrically necessary dislocations, Scr. Mater. 48 (2003) 147–153. doi:10.1016/S1359-6462(02)00358-5.

[53] J.Y. Huang, Y.T. Zhu, H. Jiang, T.C. Lowe, Microstructures and dislocation configurations in nanostructured Cu processed by repetitive corrugation and straightening, Acta Mater. 49 (2001) 1497–1505. doi:10.1016/S1359-6454(01)00069-6.

[54] C.D. Liu, M.N. Bassim, D.X. You, Dislocation structures in fatigued polycrystalline copper, Acta Metall. Mater. 42 (1994) 3695–3704. doi:10.1016/0956-7151(94)90435-9.

[55] Y.B. Lee, D.H. Shin, K.-T. Park, W.J. Nam, Effect of annealing temperature on microstructures and mechanical properties of a 5083 Al alloy deformed at cryogenic temperature, Scr. Mater. 51 (2004) 355–359. doi:10.1016/j.scriptamat.2004.02.037.